AIMS Mathematics, 10(1): 1529–1554.
DOI: 10.3934/math.2025071
Received: 28 November 2024
Revised: 08 January 2025
Accepted: 15 January 2025
Published: 23 January 2025

https://www.aimspress.com/journal/Math

Research article

Novel escape criteria for complex-valued hyperbolic functions through a fixed point iteration method

Tunçar Şahan and Yunus Atalan*

Department of Mathematics, Aksaray University, Aksaray, 68100, Türkiye

* **Correspondence:** Email: yunusatalan@aksaray.edu.tr.

Abstract: This study presented an efficient fixed-point iteration method for deriving novel escape criteria for hyperbolic sine and hyperbolic cosine functions of varying degrees. The method contributes to obtaining more accurate and effective escape criteria, thereby enhancing the mathematical understanding and computational analysis of these functions. Additionally, using the derived criteria, the iteration method was employed to generate visually appealing fractals for Julia and Mandelbrot sets, demonstrating significant advantages in computational speed and practical utility. The method's effective performance in producing complex and aesthetically satisfying fractal structures highlights its efficiency and applicability in fractal generation.

Keywords: fixed-point; iteration method; escape criterion; Julia set; Mandelbrot set
Mathematics Subject Classification: 47H10, 28A80

1. Introduction

Euclidean geometry cannot accurately represent natural shapes such as clouds or mountains in computational contexts. This limitation has been addressed through fractal geometry, derived from the Latin word "fractus," meaning broken. Fractal geometry differs fundamentally from Euclidean geometry, particularly in its characteristic self-similarity. Unlike Euclidean shapes, where close observation reveals distinct features, fractals exhibit consistent patterns at varying levels of magnification. Consequently, fractal geometry has become essential for mathematically modeling natural phenomena.

Fractals, characterized by their self-similar structures, are typically generated through iterative processes that apply specific equations or rules repeatedly. Among the most recognized fractals in the literature is the Mandelbrot set, defined by the complex function $z^2 + \mathfrak{c}$, where z is a complex variable and $\mathfrak{c} \in \mathbb{C}$ represents a complex parameter. Mandelbrot [1] observed that objects unsuitable for standard measurement exhibit a degree of roughness that often remains consistent across scales. This

roughness, quantified as the fractal dimension, enables the modeling of non-Euclidean shapes in diverse scientific disciplines. Fractals not only provide visual representations of these shapes but also facilitate precise calculations for modeling and analysis (see [2, 3]).

Recent advancements in fractal theory have significantly enhanced its applications to fractional-order systems, particularly through Caputo-like discrete fractional differences and other fractional calculus methodologies. These approaches reveal novel dynamic properties, such as non-integer symmetry, boundedness, and intricate escape-time behaviors. For example, fractional quantum Julia sets, constructed using fractional q-difference operators, exhibit distinctive fractal dynamics where parameters such as memory and scale play a critical role in shaping the fractal geometry and influencing their stability under noise perturbations. Notably, robustness to dynamic noise is quantified using tools like Julia deviation indices, demonstrating the resilience of these sets to perturbations of varying intensities [4, 5].

Similarly, spatial Julia sets generated by fractional Lotka–Volterra systems provide new perspectives on the interplay between noise and symmetry. These studies highlight how noise perturbations can disrupt the symmetrical structures of these sets, offering insights into the stability and boundedness of ecological systems. Moreover, fractional Lotka–Volterra systems enable richer dynamic behaviors than their integer-order counterparts, such as the coexistence of multiple equilibria, bifurcations, and even chaos in discrete versions [5–7].

A key advantage of fractional systems is their ability to incorporate memory effects and nonlocality, which are critical for accurately modeling complex real-world phenomena. Fractional q-difference systems provide flexibility in analyzing dynamics by adjusting parameters like scale and order, enabling precise control over fractal structures. However, challenges remain in terms of computational efficiency, particularly for systems requiring high memory depth or those influenced by strong noise [4, 5]. In contrast, fractional Lotka–Volterra systems excel in ecological modeling by providing realistic representations of predator-prey interactions, yet their sensitivity to parameter variations necessitates careful tuning and robust control strategies [6, 7]. These developments deepen the understanding of fractional-order fractals, including Julia and Mandelbrot sets, and underscore their potential applications across dynamical systems, quantum mechanics, and ecological modeling. By bridging the gaps between traditional and fractional-order systems, these studies not only enrich fractal theory but also pave the way for solving complex, nonlinear problems in diverse scientific domains [8, 9].

The relationship between fixed-point iterative methods and fractals lies in the invariance of fixed points under the mapping applied in the iterative process. These fixed points, known as attractors, draw nearby points toward them and form the structural basis of fractals. Consequently, various equations have been employed to generate fractals using fixed-point iteration methods, culminating in a rich body of literature [10–16]. For example, iterative methods applied to Julia and Mandelbrot sets enable the visualization of the complex plane, distinguishing between stable and chaotic regions through escape criteria. This visualization often involves assigning colors to points that escape to infinity, creating aesthetic patterns influenced by differences in escape velocities and the colors assigned to non-escaping points [17–19]. Such methods have found applications in engineering and physics, particularly in stability analysis, energy flow modeling, and the study of transition boundaries between order and chaos [20, 21].

Fractals generated through fixed-point iteration methods also serve practical purposes in

simulating natural phenomena, such as the geometry of coastlines or the branching of plants. These structures are integral to high-resolution graphical modeling and are used to test parallel computing algorithms and address large-scale computational challenges [22, 23]. Recent interdisciplinary applications, such as those in supply chain dynamics, further illustrate the interdisciplinary value of fractal-based methods. Julia sets, for example, have been employed to analyze the connectivity of attraction basins in dual-channel supply chains, providing insights into stability and robustness in pricing strategies. By identifying the influence of initial conditions and parameters on system stability, fractal methods aid in designing effective interventions to prevent instability caused by factors like excessive online preferences [24]. Additionally, the connectivity of Julia sets offers a framework for evaluating system robustness under varying conditions, guiding decision-making in real-world markets. These connectivity measures have informed control strategies to restore market stability, demonstrating how fractal analyses bridge mathematical theory with actionable insights in complex, multi-variable systems.

Building on these advancements, this research focuses on developing new escape criteria for hyperbolic sine and hyperbolic cosine functions. Using these criteria, the study aims to produce aesthetically satisfying fractals for Julia and Mandelbrot sets. For this purpose, a three-step, fixed-point iteration method, namely Picard-Mann-Picard (PMP), is employed due to its superior speed and practicality compared to traditional methods.

The rest of the paper is organized as follows. Section 2 provides fundamental definitions of the Mandelbrot and Julia sets, as well as the PMP fixed-point iteration method. In Section 3, escape criteria for complex-valued hyperbolic sine and hyperbolic cosine functions are derived using the PMP orbit. In Section 4, the fractal structures of the Julia and Mandelbrot sets are visualized using the PMP fixed-point iteration method. Finally, Section 5 analyzes the results and discusses future directions.

2. Preliminaries

Definition 2.1. *[25] Let $\mathfrak{p} : \mathbb{C} \to \mathbb{C}$ be a complex mapping. For any initial point $\mathfrak{z} \in \mathbb{C}$, the Picard orbit is defined as the set of iterates of $\mathfrak{z}$ as:*

$$O(\mathfrak{p}, \mathfrak{z}) = \{\mathfrak{z}_n : \mathfrak{z}_n = \mathfrak{p}(\mathfrak{z}_{n-1}), n = 1, 2, 3...\}. \tag{2.1}$$

Definition 2.2. *[26] Let $\mathbb{T} : \mathbb{C} \to \mathbb{C}$ be a complex mapping which is given by $\mathbb{T}\mathfrak{z} = \mathfrak{z}^2 + \mathfrak{c}$ for a complex parameter $\mathfrak{c} \in \mathbb{C}$. The filled Julia set is defined as:*

$$\mathbb{J}_{\mathbb{T}} = \left\{\mathfrak{z} \in \mathbb{C} : \left\{\left|\mathbb{T}^1\mathfrak{z}\right|, \left|\mathbb{T}^2\mathfrak{z}\right|, ...\right\} \textit{ is bounded}\right\}$$

in which $\left\{\mathbb{T}^i\mathfrak{z}\right\}$ is the i-th iterate of $\mathbb{T}$ and $\mathfrak{z}^2 + \mathfrak{c}$ is the boundary of $\mathbb{J}_{\mathbb{T}}$.

Definition 2.3. *[25] The Mandelbrot set $\mathbb{M}$ is defined by*

$$\mathbb{M} = \{\mathfrak{c} \in \mathbb{C} : \mathbb{J}_{\mathbb{T}} \textit{ is connected}\} \tag{2.2}$$

or equivalently,

$$\mathbb{M} = \{\mathfrak{c} \in \mathbb{C} : |\mathbb{T}\mathfrak{z}| \nrightarrow \infty \textit{ as } i \to \infty\}. \tag{2.3}$$

Definition 2.4. *[27] Let $\mathbb{T} : \mathbb{C} \to \mathbb{C}$ be a complex mapping. The PMP orbit is defined as follows for initial point $z_0 \in \mathbb{C}$:*

PMP Orbit
input: $\mathbb{T}$, $z_0 \in \mathbb{C}$, $k_n \in (0, 1]$
For $n = 0, 1, 2..., N$: ***do***
$z_{n+1} = \mathbb{T}y_n$
$y_n = (1 - k_n)\, x_n + k_n \mathbb{T}x_n$
$x_n = \mathbb{T}z_n$
end for

(2.4)

3. Main results

This section derives the escape criteria for complex-valued hyperbolic sine $\mathbb{T}(z) = a\sinh(z)^q + b(z) + \mathfrak{c}$ and hyperbolic cosine function $\mathbb{T}(z) = a\cosh(z)^q + b(z) + \mathfrak{c}$, where $q \geq 2$ and a, b, and $\mathfrak{c}$ are complex parameters, to examine the new fractal structures of Julia and Mandelbrot sets by using the PMP iteration method.

3.1. Escape criteria for $\mathbb{T}(z) = a\sinh(z)^q + b(z) + \mathfrak{c}$

The following expression establishes

$$\begin{aligned} |\sinh(z^q)| &= \left|\sum_{n=0}^{\infty} \frac{z^{q(2n+1)}}{(2n+1)!}\right| \\ &= \left|z^q + \frac{z^{3q}}{3!} + \frac{z^{5q}}{5!} + \cdots\right| \\ &= \left|z^q\left(1 + \frac{z^{2q}}{3!} + \frac{z^{4q}}{5!} + \cdots\right)\right| \\ &= |z^q|\left|1 + \frac{z^{2q}}{3!} + \frac{z^{4q}}{5!} + \cdots\right| \\ &\geq |z^q|\,|\hbar_1| \end{aligned} \tag{3.1}$$

in which $|\hbar_1| \in (0, 1]$ and $|\hbar_1| \leq \left|1 + \frac{z^{2q}}{3!} + \frac{z^{4q}}{5!} + \cdots\right| = \left|\sum_{n=1}^{\infty} \frac{z^{q(2n)}}{(2n+1)!}\right|$.

In the same way, we get $|\sinh(y^q)| \geq |y^q|\,|\hbar_2|$ in which $|\hbar_2| \in (0, 1]$ and $|\hbar_2| \leq \left|\sum_{n=1}^{\infty} \frac{y^{q(2n)}}{(2n+1)!}\right|$; and $|\sinh(x^q)| \geq |x^q|\,|\hbar_3|$ in which $|\hbar_3| \in (0, 1]$ and $|\hbar_3| \leq \left|\sum_{n=1}^{\infty} \frac{x^{q(2n)}}{(2n+1)!}\right|$.

Theorem 3.1. *Assume that $\mathbb{T}(z) = a\sinh(z)^q + bz + \mathfrak{c}$, $q \geq 2$, and*

$$|z| \geq |\mathfrak{c}| > \max\left\{\left(\frac{2 + |b|}{|a|\,|\hbar_1|}\right)^{\frac{1}{q-1}}, \left(\frac{2 + |b|}{|a|\,|\hbar_2|}\right)^{\frac{1}{q-1}}, \left(\frac{2 + |b|}{k\,|a|\,|\hbar_3|}\right)^{\frac{1}{q-1}}\right\}$$

in which $0 < k < 1$ *and* $\mathfrak{c} \in \mathbb{C}$. *Let* $\{z_n\}_{n=0}^{\infty}$ *be an iterative sequence generated by PMP orbit (2.4) by taking* $z_0 = z, y_0 = y, x_0 = x$, *and* $k_n = k$ *as under:*

PMP Iteration Method
input: $\mathbb{T}$, $z_0 \in \mathbb{C}$, $k \in (0, 1]$
For $n = 0, 1, 2..., N$: ***do***
$z_{n+1} = \mathbb{T}y_n$
$y_n = (1-k)\, x_n + k\mathbb{T}x_n$
$x_n = \mathbb{T}z_n$
end for

(3.2)

Then $|z_n| \to \infty$ *as* $n \to \infty$.

Proof. Consider

$$\begin{aligned} |x| = |\mathbb{T}z| &= |a\sinh(z)^q + bz + \mathfrak{c}| \\ &\geq |a\sinh(z)^q + bz| - |\mathfrak{c}| \\ &\geq |a\sinh(z)^q| - |bz| - |\mathfrak{c}| \\ &= |a|\,|\sinh(z)^q| - |b|\,|z| - |\mathfrak{c}| \end{aligned} \tag{3.3}$$

and by using $|z| \geq |\mathfrak{c}|$ and (3.1), we get

$$|x| \geq a\,|z^q|\,|\hbar_1| - |b|\,|z| - |z| = |z|\left(|a|\left|z^{q-1}\right|\,|\hbar_1| - (|b|+1)\right). \tag{3.4}$$

From the assumptions, we have

$$|z| > \left(\frac{2+|b|}{|a|\,|\hbar_1|}\right)^{\frac{1}{q-1}} \Leftrightarrow |z|^{q-1} > \left(\frac{2+|b|}{|a|\,|\hbar_1|}\right) \Leftrightarrow |z|^{q-1}\,|a|\,|\hbar_1| > 2 + |b|\,.$$

That is, we obtain $|z|^{q-1}\,|a|\,|\hbar_1| - (|b|+1) > 1$. Hence, from (3.4), we get

$$|x| > |z|\,. \tag{3.5}$$

Similarly,

$$\begin{aligned} |y| &= |(1-k)\, x + k\mathbb{T}x| \\ &= |(1-k)\, x + k\,(a\sinh(x)^q + bx + \mathfrak{c})| \\ &\geq |(1-k)\, x + k\,(a\sinh(x)^q + bx)| - k\,|\mathfrak{c}| \\ &\geq |(1-k)\, x + k\,(a\sinh(x)^q + bx)| - k\,|z| \quad (\text{since } |z| \geq |\mathfrak{c}|) \\ &> |(1-k)\, z + k\,(a\sinh(x)^q + bz)| - k\,|z| \quad (\text{since } |x| > |z|) \\ &\geq |k\,(a\sinh(x)^q + bz)| - (1-k)\,|z| - k\,|z| \\ &\geq |k\,(a\sinh(x)^q)| - (1-k)\,|z| - k\,|b|\,|z| - k\,|z| \\ &\geq |k\,(a\sinh(x)^q)| - |b|\,|z| - |z| \quad (\text{since } |b|\,|z| > k\,|b|\,|z|) \end{aligned}$$

$$= k\,|a|\,|\sinh(x)^q| - |b|\,|z| - |z|\,.$$

Since $|\sinh(x^q)| \geq |x^q|\,|\hbar_3|$, we get

$$\begin{aligned} |y| &\geq k\,|a|\,|x^q|\,|\hbar_3| - |b|\,|z| - |z| \\ &> k\,|a|\,|z^q|\,|\hbar_3| - |b|\,|z| - |z| \quad (\text{since } |x| > |z|) \\ &= |z|\left(k\,|a|\left|z^{q-1}\right|\,|\hbar_3| - (|b|+1)\right). \end{aligned} \tag{3.6}$$

From the assumptions, we have

$$|z| > \left(\frac{2+|b|}{k\,|a|\,|\hbar_3|}\right)^{\frac{1}{q-1}} \Leftrightarrow |z|^{q-1} > \left(\frac{2+|b|}{k\,|a|\,|\hbar_3|}\right) \Leftrightarrow |z|^{q-1}\,k\,|a|\,|\hbar_3| > 2 + |b|\,.$$

So, we have $|z|^{q-1}\,k\,|a|\,|\hbar_3| - (|b|+1) > 1$. Hence, from (3.6), we get

$$|y| > |z|\,. \tag{3.7}$$

For the last step of (3.2),

$$\begin{aligned} |z_1| &= |a\sinh(y)^q + by + \mathfrak{c}| \\ &\geq |a\sinh(y)^q + by| - |\mathfrak{c}| \\ &\geq |a\sinh(y)^q + by| - |z| \quad (\text{since } |z| \geq |c|) \\ &> |a\sinh(y)^q + bz| - |z| \quad (\text{since } |y| > |z|) \\ &> |a\sinh(y)^q| - |b|\,|z| - |z| \\ &= |a|\,|\sinh(y)^q| - |b|\,|z| - |z|\,. \end{aligned} \tag{3.8}$$

Since $|\sinh(y^q)| \geq |y^q|\,|\hbar_2|$, we get

$$\begin{aligned} |z_1| &\geq |a|\,|y^q|\,|\hbar_2| - |b|\,|z| - |z| \\ &> |a|\,|z^q|\,|\hbar_2| - |b|\,|z| - |z| \quad (\text{since } |y| > |z|) \\ &= |z|\left(|a|\left|z^{q-1}\right|\,|\hbar_2| - (|b|+1)\right). \end{aligned} \tag{3.9}$$

We also have

$$|z_2| > |z_1|\left(|a|\left|z^{q-1}\right|\,|\hbar_2| - (|b|+1)\right) > |z|\left(|a|\left|z^{q-1}\right|\,|\hbar_2| - (|b|+1)\right)^2.$$

Iterating this process n-times, we have

$$\begin{aligned} |z_3| &> |z|\left(|a|\left|z^{q-1}\right|\,|\hbar_2| - (|b|+1)\right)^3 \\ |z_4| &> |z|\left(|a|\left|z^{q-1}\right|\,|\hbar_2| - (|b|+1)\right)^4 \\ &\vdots \\ |z_n| &> |z|\left(|a|\left|z^{q-1}\right|\,|\hbar_2| - (|b|+1)\right)^n. \end{aligned}$$

From the assumptions, we have

$$|z| > \left(\frac{2+|b|}{|a|\,|\hbar_2|}\right)^{\frac{1}{q-1}} \Leftrightarrow |z|^{q-1} > \left(\frac{2+|b|}{|a|\,|\hbar_2|}\right) \Leftrightarrow |z|^{q-1}\,|a|\,|\hbar_2| > 2+|b|\,.$$

Thus

$$|z|^{q-1}\,|a|\,|\hbar_2| - (|b|+1) > 1.$$

Then, we get

$$|z_n| > |z|\,.$$

Thus, $|z_n| \to \infty$ as $n \to \infty$. □

Corollary 3.1. *Suppose that*

$$|z_n| \geq \max\left\{|\mathfrak{c}|\,, \left(\frac{2+|b|}{|a|\,|\hbar_1|}\right)^{\frac{1}{q-1}}, \left(\frac{2+|b|}{|a|\,|\hbar_2|}\right)^{\frac{1}{q-1}}, \left(\frac{2+|b|}{k\,|a|\,|\hbar_3|}\right)^{\frac{1}{q-1}}\right\}.$$

Because of $|z|^{q-1}\,|a|\,|\hbar_2| - (|b|+1) > 1$ *and* $\left|z_{n+p}\right| > |z|\left(|a|\left|z^{q-1}\right|\,|\hbar_2| - (|b|+1)\right)^{n+p}$, *then* $|z_n| \to \infty$ *as* $n \to \infty$.

3.2. Escape criteria for $\mathbb{T}(z) = a\cosh(z)^q + bz + \mathfrak{c}$

$$\begin{aligned} |\cosh(z^q)| &= \left|\sum_{n=0}^{\infty} \frac{z^{q(2n)}}{(2n)!}\right| \\ &= \left|1 + \frac{z^{2q}}{2!} + \frac{z^{4q}}{4!} + \cdots\right| \\ &> \left|\frac{z^{2q}}{2!} + \frac{z^{4q}}{4!} + \cdots\right| \\ &= |z^q|\left|\frac{z^q}{2!} + \frac{z^{3q}}{4!} + \cdots\right| \\ &\geq |z^q|\,|\wp_1| \end{aligned} \tag{3.10}$$

in which $|\wp_1| \in (0,1]$ and $|\wp_1| \leq \left|\frac{z^q}{2!} + \frac{z^{3q}}{4!} + \cdots\right| = \left|\sum_{n=1}^{\infty} \frac{z^{q(2n-1)}}{(2n)!}\right|$.

In the same way, we get $|\cosh(y^q)| \geq |y^q|\,|\wp_2|$ in which $|\wp_2| \in (0,1]$ and $|\wp_2| \leq \left|\sum_{n=1}^{\infty} \frac{y^{q(2n-1)}}{(2n)!}\right|$; and $|\cosh(x^q)| \geq |x^q|\,|\wp_3|$ in which $|\wp_3| \in (0,1]$ and $|\wp_3| \leq \left|\sum_{n=1}^{\infty} \frac{x^{q(2n-1)}}{(2n)!}\right|$.

Theorem 3.2. *Assume that* $\mathbb{T}(z) = a\cosh(z)^q + b(z) + \mathfrak{c}$, $q \geq 2$, *and*

$$|z| \geq |\mathfrak{c}| > \max\left\{\left(\frac{2+|b|}{|a|\,|\wp_1|}\right)^{\frac{1}{q-1}}, \left(\frac{2+|b|}{|a|\,|\wp_2|}\right)^{\frac{1}{q-1}}, \left(\frac{2+|b|}{k\,|a|\,|\wp_3|}\right)^{\frac{1}{q-1}}\right\}$$

in which $0 < k < 1$ *and* $\mathfrak{c} \in \mathbb{C}$. *Let* $\{z_n\}_{n=1}^{\infty}$ *be an iterative sequence generated by (3.2). Then* $|z_n| \to \infty$ *as* $n \to \infty$.

Proof. Consider

$$\begin{aligned} |x| = |\mathbb{T}z| &= |a\cosh(z)^q + bz + \mathfrak{c}| \\ &\geq |a\cosh(z)^q + bz| - |\mathfrak{c}| \\ &\geq |a\cosh(z)^q| - |bz| - |\mathfrak{c}| \\ &= |a|\,|\cosh(z)^q| - |b|\,|z| - |\mathfrak{c}| \end{aligned} \tag{3.11}$$

and by using $|z| \geq |\mathfrak{c}|$ and (3.10), we get

$$\begin{aligned} |x| &\geq a\,|z^q|\,|\wp_1| - |b|\,|z| - |z| \\ &= |z|\left(|a|\left|z^{q-1}\right|\,|\wp_1| - (|b|+1)\right). \end{aligned} \tag{3.12}$$

From the assumptions, we have

$$|z| > \left(\frac{2+|b|}{|a|\,|\wp_1|}\right)^{\frac{1}{q-1}} \Leftrightarrow |z|^{q-1} > \left(\frac{2+|b|}{|a|\,|\wp_1|}\right) \Leftrightarrow |z|^{q-1}\,|a|\,|\wp_1| > 2 + |b|\,.$$

That is, we obtain

$$|z|^{q-1}\,|a|\,|\wp_1| - (|b|+1) > 1.$$

Hence, from (3.12), we get

$$|x| > |z|\,. \tag{3.13}$$

Similarly,

$$\begin{aligned} |y| &= |(1-k)\,x + k\mathbb{T}x| \\ &= |(1-k)\,x + k\,(a\cosh(x)^q + bx + \mathfrak{c})| \\ &\geq |(1-k)\,x + k\,(a\cosh(x)^q + bx)| - k\,|\mathfrak{c}| \\ &\geq |(1-k)\,x + k\,(a\cosh(x)^q + bx)| - k\,|z| \quad (\text{since } |z| \geq |\mathfrak{c}|) \\ &> |(1-k)\,z + k\,(a\cosh(x)^q + bz)| - k\,|z| \quad (\text{since } |x| > |z|) \\ &\geq |k\,(a\cosh(x)^q + bz)| - (1-k)\,|z| - k\,|z| \\ &\geq |k\,(a\cosh(x)^q)| - (1-k)\,|z| - k\,|b|\,|z| - k\,|z| \\ &\geq |k\,(a\cosh(x)^q)| - |b|\,|z| - |z| \quad (\text{since } |b|\,|z| > k\,|b|\,|z|) \\ &= k\,|a|\,|\cosh(x)^q| - |b|\,|z| - |z|\,. \end{aligned}$$

Since $|\cosh(x^q)| \geq |x^q|\,|\wp_3|$, we get

$$\begin{aligned} |y| &\geq k\,|a|\,|x^q|\,|\wp_3| - |b|\,|z| - |z| \\ &> k\,|a|\,|z^q|\,|\wp_3| - |b|\,|z| - |z| \quad (\text{since } |x| > |z|) \\ &= |z|\left(k\,|a|\left|z^{q-1}\right|\,|\wp_3| - (|b|+1)\right). \end{aligned} \tag{3.14}$$

From the assumptions, we have

$$|z| > \left(\frac{2+|b|}{k\,|a|\,|\wp_3|}\right)^{\frac{1}{q-1}} \Leftrightarrow |z|^{q-1} > \left(\frac{2+|b|}{k\,|a|\,|\wp_3|}\right) \Leftrightarrow |z|^{q-1}\,k\,|a|\,|\wp_3| > 2 + |b|\,.$$

So, we have

$$|z|^{q-1}\, k\, |a|\, |\wp_3| - (|b|+1) > 1.$$

Hence, from (3.14), we get

$$|y| > |z|\,. \tag{3.15}$$

For the last step of (3.2),

$$\begin{aligned} |z_1| &= |a\cosh(y)^q + by + \mathfrak{c}| \\ &\geq |a\cosh(y)^q + by| - |\mathfrak{c}| \\ &\geq |a\cosh(y)^q + by| - |z| \quad (\text{since } |z| \geq |\mathfrak{c}|) \\ &> |a\cosh(y)^q + bz| - |z| \quad (\text{since } |y| > |z|) \\ &> |a\cosh(y)^q| - |b|\,|z| - |z| \\ &= |a|\,|\cosh(y)^q| - |b|\,|z| - |z|\,. \end{aligned} \tag{3.16}$$

Since $|\cosh(y^q)| \geq |y^q|\,|\wp_2|$, we get

$$\begin{aligned} |z_1| &\geq |a|\,|y^q|\,|\wp_2| - |b|\,|z| - |z| \\ &> |a|\,|z^q|\,|\wp_2| - |b|\,|z| - |z| \quad (\text{since } |y| > |z|) \\ &= |z|\left(|a|\left|z^{q-1}\right|\,|\wp_2| - (|b|+1)\right). \end{aligned} \tag{3.17}$$

We also get

$$|z_2| > |z_1|\left(|a|\left|z^{q-1}\right|\,|\wp_2| - (|b|+1)\right) > |z|\left(|a|\left|z^{q-1}\right|\,|\wp_2| - (|b|+1)\right)^2.$$

Iterating this process n-times, we have

$$\begin{aligned} |z_3| &> |z|\left(|a|\left|z^{q-1}\right|\,|\wp_2| - (|b|+1)\right)^3 \\ |z_4| &> |z|\left(|a|\left|z^{q-1}\right|\,|\wp_2| - (|b|+1)\right)^4 \\ &\vdots \\ |z_n| &> |z|\left(|a|\left|z^{q-1}\right|\,|\wp_2| - (|b|+1)\right)^n. \end{aligned}$$

From the assumptions, we have

$$|z| > \left(\frac{2+|b|}{|a|\,|\wp_2|}\right)^{\frac{1}{q-1}} \Leftrightarrow |z|^{q-1} > \left(\frac{2+|b|}{|a|\,|\wp_2|}\right) \Leftrightarrow |z|^{q-1}\,|a|\,|\wp_2| > 2+|b|\,.$$

Thus,

$$|z|^{q-1}\,|a|\,|\wp_2| - (|b|+1) > 1.$$

Then, we get $|z_n| > |z|$. Hence, $|z_n| \to \infty$ as $n \to \infty$. □

Corollary 3.2. *Suppose that*

$$|z_n| \geq \max\left\{|\mathfrak{c}|, \left(\frac{2+|b|}{|a|\,|\wp_1|}\right)^{\frac{1}{q-1}}, \left(\frac{2+|b|}{|a|\,|\wp_2|}\right)^{\frac{1}{q-1}}, \left(\frac{2+|b|}{k\,|a|\,|\wp_3|}\right)^{\frac{1}{q-1}}\right\}.$$

Because of

$$|z|^{q-1}\,|a|\,|\wp_2| - (|b|+1) > 1$$

and

$$\left|z_{n+p}\right| > |z|\left(|a|\left|z^{q-1}\right|\,|\wp_2| - (|b|+1)\right)^{n+p},$$

then $|z_n| \to \infty$ *as* $n \to \infty$.

4. Construction of fractals

In this section, some aesthetically pleasing fractals were generated for complex-valued hyperbolic sine and hyperbolic cosine functions via PMP iteration method (3.2). The algorithms were implemented in MATLAB® R2022a, and the experiments were performed on a computer with the following specifications: Intel Core i5-7400 CPU @ 3.00 GHz, 8 GB DDR4 RAM, and Microsoft Windows 11 Pro (64-bit).

4.1. Julia sets

The parameter tables for the Julia sets generated by Algorithms 1 and 2 are presented below.

Algorithm 1: The Julia set for the hyperbolic sine function

input: $\mathbb{T}(z) = a\sinh(z)^q + bz + \mathfrak{c}$, $a, b, \mathfrak{c} \in \mathbb{C}$, $q \geq 2$, $A \subset \mathbb{C}$-occupied area, $k \in (0, 1]$, $\mathbb{P}$ is the maximum number of iterations;
Output: Julia set for occupied area A
For $z_0 \in A$: **do**
$C_1 = \left(\frac{2+|b|}{|a||\hbar_1|}\right)^{\frac{1}{q-1}}$, $C_2 = \left(\frac{2+|b|}{|a||\hbar_2|}\right)^{\frac{1}{q-1}}$, $C_3 = \left(\frac{2+|b|}{k|a||\hbar_3|}\right)^{\frac{1}{q-1}}$,
$C = \max\{|\mathfrak{c}|, C_1, C_2, C_3\}$, $n = 0$, $z_0 = 0$
while $n \geq \mathbb{P}$ **do**
$x_n = \mathbb{T}z_n$, $y_n = (1-k)\,x_n + k\mathbb{T}x_n$, $z_{n+1} = \mathbb{T}y_n$
if $|z_{n+1}| > C$ **then**
break
end if
$n = n + 1$
end while
end for

Algorithm 2: The Julia set for the hyperbolic cosine function

input: $\mathbb{T}(z) = a\cosh(z)^q + bz + \mathfrak{c}$, $a, b, \mathfrak{c} \in \mathbb{C}$, $q \geq 2$, $A \subset \mathbb{C}$-occupied area, $k \in (0, 1]$, $\mathbb{P}$ is the maximum number of iterations;

Output: Julia set for occupied area A

For $z_0 \in A$: **do**

$C_1 = \left(\frac{2+|b|}{|a||\wp_1|}\right)^{\frac{1}{q-1}}$, $C_2 = \left(\frac{2+|b|}{|a||\wp_2|}\right)^{\frac{1}{q-1}}$, $C_3 = \left(\frac{2+|b|}{k|a||\wp_3|}\right)^{\frac{1}{q-1}}$,

$C = \max\{|\mathfrak{c}|, C_1, C_2, C_3\}$, $n = 0$, $z_0 = 0$

while $n \geq \mathbb{P}$ **do**

$x_n = \mathbb{T}z_n$, $y_n = (1-k)\,x_n + k\mathbb{T}x_n$, $z_{n+1} = \mathbb{T}y_n$

if $|z_{n+1}| > C$ **then**

break

end if

$n = n + 1$

end while

end for

Figure 1(a) This fractal, defined within the range $[-3, 3] \times [-3, 3]$, was generated in 1.916 seconds. It exhibits symmetry with respect to the x-axis, a hallmark of classical Julia sets. The edges of the fractal display softer color transitions and lower density, whereas the central region features increased intensity and complexity. This contrast reflects the inherent characteristics of Julia sets, where boundary regions are less repetitive and therefore less prominent. The relatively short computation time suggests a lower density of intricate details within the selected range compared to subsequent figures.

Figure 1(b) Defined in the range $[-3.5, 3.5] \times [-3, 3]$, this fractal required 3.259 seconds to generate. The symmetry about the x-axis persists, while the extended horizontal axis introduces greater detail and complexity in the peripheral regions. The sharper color transitions near the edges contrast with the denser color gradients in the central region, highlighting the intricate structure of the Julia set. The broader domain necessitated more extensive computations, leading to an increase in generation time compared to Figure 1(a).

Figure 1(c) This fractal, confined to the range $[-2.5, 2.5] \times [-3, 3]$, was generated in 4.043 seconds. The narrowed horizontal domain emphasizes finer details, particularly in the central region, where color gradients intensify significantly. Symmetrical and well-defined features are evident along the edges, underscoring the dynamic structures characteristic of Julia sets at their boundary regions. The extended computation time reflects the higher resolution and increased density of details resulting from the reduced range.

Figure 1(d) Defined within the range $[-2.5, 2.5] \times [-2.5, 2.5]$, this fractal was produced in 3.710 seconds. The reduced range along both axes yields a more homogeneous distribution of details,

enhancing the symmetry of the fractal's structure. The central regions exhibit sharper color gradients, while the edges display smoother transitions. The narrower domain reduces the overall computational burden compared to Figure 1(c), resulting in a slight decrease in generation time despite the high resolution of the details.

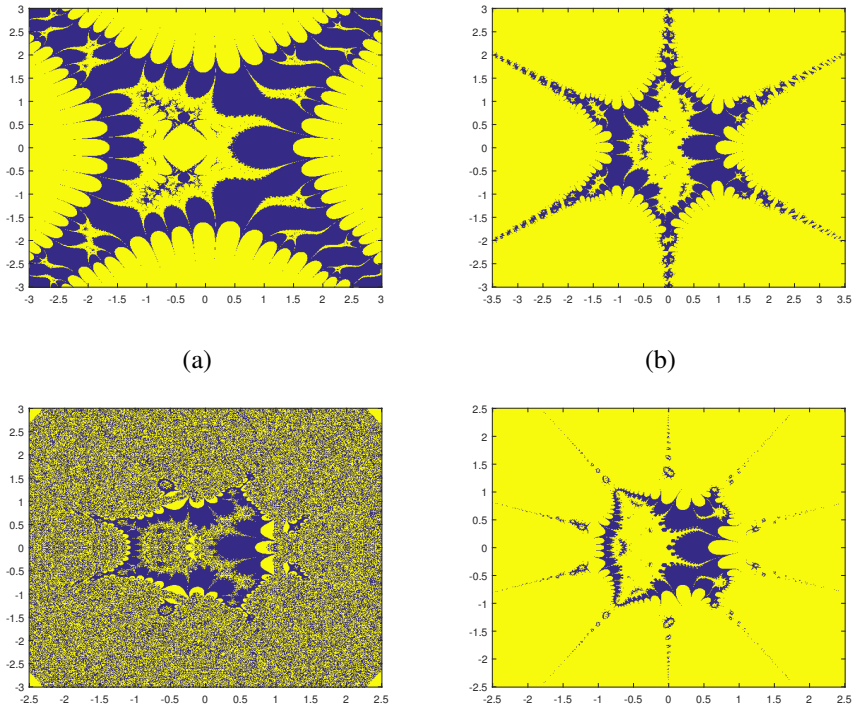

(a) (b)

(c) (d)

Figure 1. Fractals obtained from the Julia set according to the q values in Table 1.

Table 1. The parameters applied in Figure 1.

Fig. No	a	b	$\mathfrak{c}$	k	$\hbar_1$	$\hbar_2$	$\hbar_3$	q
1(a)	3.1	2.2	1.3	0.0009	0.0005	0.0004	0.0003	2
1(b)	3.1	2.2	1.3	0.0009	0.0005	0.0004	0.0003	3
1(c)	3.1	2.2	1.3	0.0009	0.0005	0.0004	0.0003	4
1(d)	3.1	2.2	1.3	0.0009	0.0005	0.0004	0.0003	5

Figure 2(a) This fractal exhibits a structure strongly reminiscent of classical Julia sets, characterized by intricate patterns and sharp boundaries. The fractal demonstrates perfect symmetry along both horizontal and vertical axes, reflecting a balanced geometric composition. Defined within the range $[-2, 2] \times [-2, 2]$, it was generated in 1.986 seconds, highlighting the efficiency of the computational algorithm. The color intensity peaks near the center and gradually diminishes toward the edges, signifying a concentration of iterations in the central regions.

Figure 2(b) This fractal bears similarities to the Mandelbrot set, displaying a broader and more expansive structure. The fractal is perfectly symmetric about its central axis, presenting a visually striking equilibrium. Spanning the range $[-3, 3] \times [-3, 3]$, this shape was produced in 1.992 seconds, showcasing the algorithm's capability to handle larger domains effectively. The color intensity is most pronounced at the center, fading progressively toward the periphery, indicating a decline in iteration density with increasing distance from the core.

Figure 2(c) This fractal deviates from classical Julia sets with its asymmetrical configuration, exhibiting symmetry along the horizontal axis but a slight asymmetry along the vertical axis, resulting in a distinctive form. Defined over the range $[-3, 2.5] \times [-2, 2]$, this fractal required 2.026 seconds for generation, suggesting that its complexity has a noticeable impact on computational time. The color intensity features abrupt transitions and dramatic variations in certain regions, highlighting the dynamic and variable nature of the iteration process.

Figure 2(d) This fractal presents a compact and dense structure, distinguishing itself from more traditional Julia sets. While it maintains symmetry along the vertical axis, it lacks complete symmetry along the horizontal axis. Defined within the restricted range $[-2, 2] \times [-1, 1]$, it was generated in 1.995 seconds, illustrating the computational advantage of a smaller domain. The color intensity is markedly high at the center and diminishes significantly toward the edges, underscoring the concentration of iterations near the central area.

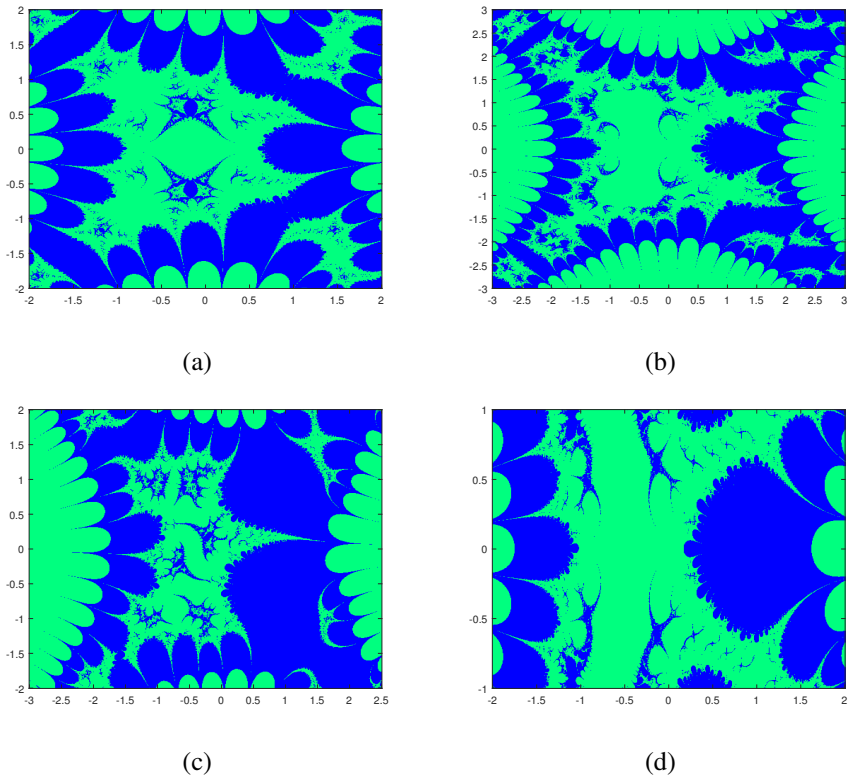

(a) (b)

(c) (d)

Figure 2. Fractals obtained from the Julia set for varying values of all parameters except q according to Table 2.

Table 2. The parameters applied in Figure 2.

Fig. No	a	b	$\mathfrak{c}$	k	$\hbar_1$	$\hbar_2$	$\hbar_3$	q
2(a)	3+0.0005i	1+0.0004i	1+0.0004i	0.0005	0.0003	0.0004	0.0005	2
2(b)	1+0.0001i	1-0.0002i	2+0.0003i	0.0030	0.0090	0.0095	0.0065	2
2(c)	-1+1.8i	-1+1.5i	-2+2.4i	0.0088	0.0011	0.0022	0.0033	2
2(d)	2+0.004i	2+0.003i	2+0.005i	0.0034	0.0023	0.0044	0.0024	2

Figure 3(a) This fractal demonstrates characteristics commonly associated with Julia sets, particularly in its intricate and recursive structures. It exhibits perfect symmetry along both horizontal and vertical axes, creating a balanced and aesthetically pleasing geometry. Defined over the range $[-3,3]\times[-3,3]$, it was generated in 2.021 seconds, reflecting efficient computation for a relatively large domain. The color intensity is concentrated near the center and diminishes toward the periphery, indicating a high density of iterations in central regions.

Figure 3(b) This fractal retains similarities to traditional Julia sets but introduces a more compact and localized structure. It showcases vertical and horizontal symmetry, though with a slightly distorted balance compared to Figure 3(a). Defined within $[-2.5,2]\times[-2,2]$, the generation time was 3.249 seconds, longer than Figure 3(a), possibly due to increased computational complexity in parameter adjustments. The color intensity features smooth transitions, with a gradual fade from the center outward, highlighting the iterative concentration in central zones.

Figure 3(c) This fractal deviates from the traditional Julia sets by presenting a denser and more confined structure. It is symmetric along both axes, maintaining a sense of equilibrium and uniformity. Defined over $[-2,2]\times[-2,2]$, this fractal required 3.995 seconds for generation, suggesting that its compact form and parameter intricacies added to the computational load. The color intensity is highly concentrated in certain regions, with sharp variations that emphasize the dynamic effects of iterative processes.

Figure 3(d) This fractal offers a broader and more intricate configuration compared to the others, resembling a hybrid of Julia and Mandelbrot set characteristics. It exhibits near-perfect symmetry along both axes, contributing to its visually compelling design. Defined within the range $[-2.5,2.5]\times[-2.5,2.5]$, it was generated in 3.978 seconds, reflecting the computational demands of its complex and detailed structure. The color intensity varies smoothly across the fractal, with higher concentrations near the center and subtler gradients extending outward, illustrating the influence of the underlying iterative dynamics.

Table 3. The parameters applied in Figure 3.

Fig. No	a	b	$\mathfrak{c}$	k	$\wp_1$	$\wp_2$	$\wp_3$	q
3(a)	2.0009	0.0001	0.0002	0.0080	0.70	0.80	0.90	2
3(b)	2.0009	0.0001	0.0002	0.0080	0.70	0.80	0.90	3
3(c)	2.0009	0.0001	0.0002	0.0080	0.70	0.80	0.90	4
3(d)	2.0009	0.0001	0.0002	0.0080	0.70	0.80	0.90	5

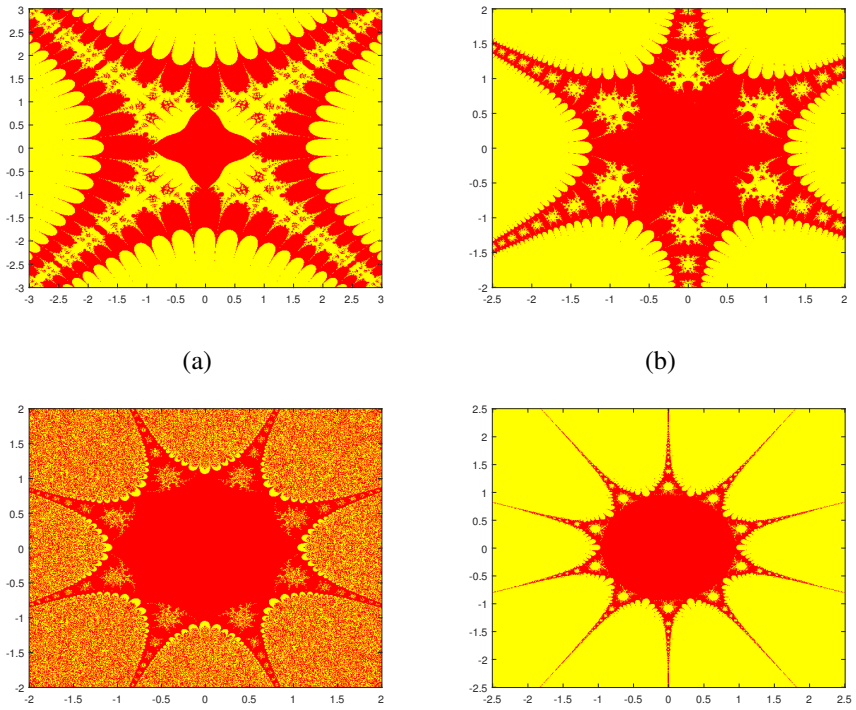

(a) (b)

(c) (d)

Figure 3. Fractals obtained from the Julia set according to the q values in Table 3.

Figure 4(a) The fractal depicted in Figure 4(a) corresponds to a Julia set defined within the range $[-1, 1] \times [-2, 2]$. This structure demonstrates a strong resemblance to classical Julia sets, characterized by intricate branching patterns and self-similar geometries. The configuration exhibits bilateral symmetry with respect to the vertical axis, which enhances its visual regularity. The computational process required 2.038 seconds, suggesting efficient rendering within this constrained range. Color gradients in this representation emphasize the complexity of its boundaries, highlighting regions of high iterative density.

Figure 4(b) This fractal presents a Julia set generated over a broader area, $[-2, 2] \times [-3, 3]$. This fractal maintains key features of traditional Julia sets, including recursive branching and intricate edge structures. Notably, the symmetry extends across both horizontal and vertical axes, creating a balanced and harmonious visual pattern. The computation time of 2.011 seconds indicates a comparable efficiency despite the expanded domain. The distribution of color intensities reveals intricate transitions between regions of high and low iteration counts, enriching the fractal's aesthetic appeal.

Figure 4(c) The fractal illustrated here spans the range $[-2.5, 2.5] \times [-2.5, 2.5]$, further extending the spatial domain. This Julia set diverges slightly from strict axial symmetry, instead showcasing localized symmetries around its central region. The rendering required 2.037 seconds, consistent with the computational times observed in smaller domains. The color scheme underscores the fine-grained complexity of the structure, particularly in areas where iterative behaviors shift rapidly, offering a dynamic and textured visual experience.

Figure 4(d) This fractal features a Julia set defined over the range $[-3, 3] \times [-2, 2]$, the largest domain among the analyzed shapes. While the fractal exhibits horizontal asymmetry in its global structure, local symmetries persist, especially near prominent features. The computation time of 2.025 seconds highlights the scalability of the generation algorithm across varying domain sizes. The variation in color intensity accentuates the fractal's intricate edges and inner patterns, reinforcing the depth and richness of its geometry.

Table 4. The parameters applied in Figure 4.

Fig. No	a	b	$\mathfrak{c}$	k	$\wp_1$	$\wp_2$	$\wp_3$	q
4(a)	2+0.001i	0.0001+0.0001i	0.002+0.002i	0.0010	0.0004	0.0008	0.0016	2
4(b)	2+0.005i	0.05-0.001i	0.06+0.002i	0.0020	0.0022	0.0024	0.0026	2
4(c)	2i	0.1i	0.2i	0.030	0.10	0.20	0.30	2
4(d)	2+0.02i	0.001i	0.0011+0.0003i	0.0040	0.42	0.44	0.46	2

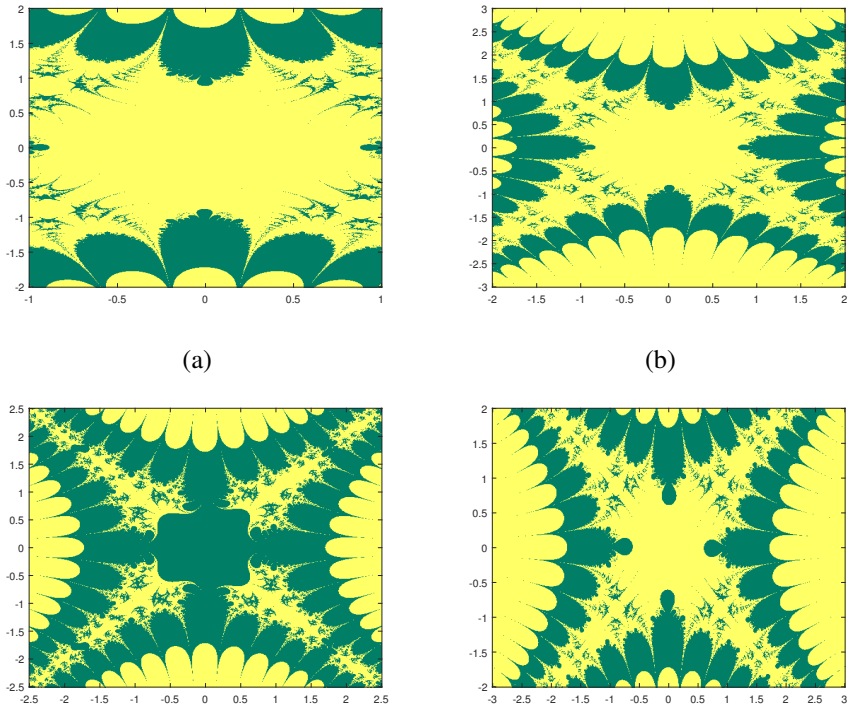

(a) (b)

(c) (d)

Figure 4. Fractals obtained from the Julia set for varying values of all parameters except q according to Table 4.

4.2. Mandelbrot sets

The parameter tables for the Mandelbrot sets generated by Algorithms 3 and 4 are presented below.

Algorithm 3: The Mandelbrot set for the hyperbolic sine function

input: $\mathbb{T}(z) = a\sinh(z)^q + bz + \mathfrak{c}$, $a, b, \mathfrak{c} \in \mathbb{C}$, $q \geq 2$, $A \subset \mathbb{C}$-occupied area, $k \in (0, 1]$, $\mathbb{P}$ is the maximum number of iterations;

Output: Mandelbrot set for occupied area A

For $z_0 \in A$: **do**

$C_1 = \left(\frac{2+|b|}{|a||\hbar_1|}\right)^{\frac{1}{q-1}}$, $C_2 = \left(\frac{2+|b|}{|a||\hbar_2|}\right)^{\frac{1}{q-1}}$, $C_3 = \left(\frac{2+|b|}{k|a||\hbar_3|}\right)^{\frac{1}{q-1}}$,

$C = \max\{|\mathfrak{c}|, C_1, C_2, C_3\}$, $n = 0$, $z_0 = 0$

while $n \geq \mathbb{P}$ **do**

$x_n = \mathbb{T}z_n$, $y_n = (1-k)\,x_n + k\mathbb{T}x_n$, $z_{n+1} = \mathbb{T}y_n$

if $|z_{n+1}| > C$ **then**

break

end if

$n = n + 1$

end while

end for

Algorithm 4: The Mandelbrot set for the hyperbolic cosine function

input: $\mathbb{T}(z) = a\cosh(z)^q + bz + \mathfrak{c}$, $a, b, \mathfrak{c} \in \mathbb{C}$, $q \geq 2$, $A \subset \mathbb{C}$-occupied area, $k \in (0, 1]$, $\mathbb{P}$ is the maximum number of iterations;

Output: Mandelbrot set for occupied area A

For $z_0 \in A$: **do**

$C_1 = \left(\frac{2+|b|}{|a||\wp_1|}\right)^{\frac{1}{q-1}}$, $C_2 = \left(\frac{2+|b|}{|a||\wp_2|}\right)^{\frac{1}{q-1}}$, $C_3 = \left(\frac{2+|b|}{k|a||\wp_3|}\right)^{\frac{1}{q-1}}$,

$C = \max\{|\mathfrak{c}|, C_1, C_2, C_3\}$, $n = 0$, $z_0 = 0$

while $n \geq \mathbb{P}$ **do**

$x_n = \mathbb{T}z_n$, $y_n = (1-k)\,x_n + k\mathbb{T}x_n$, $z_{n+1} = \mathbb{T}y_n$

if $|z_{n+1}| > C$ **then**

break

end if

$n = n + 1$

end while

end for

Figure 5(a) This fractal exhibits the classical features of the Mandelbrot set, characterized by its distinct branching structures and symmetric geometry. Defined within the range $[-2, 2] \times [-3, 3]$, the fractal demonstrates clear symmetry along both the horizontal and vertical axes. The computation time for this figure was 2.025 seconds, reflecting a relatively efficient

generation process. The color intensity transitions smoothly outward from the center, emphasizing the intricate complexity of the set and enhancing visual clarity for detailed analysis.

Figure 5(b) This fractal, defined over the extended range of $[-2.5, 2.5] \times [-3, 3]$, provides a more detailed visualization of the Mandelbrot set's familiar structures. Its symmetry is particularly evident in the branching patterns concentrated near the center. The figure required 3.322 seconds for generation, a notable increase due to the broader domain. The variation in color intensity effectively highlights the intricate internal structures, facilitating in-depth visual and computational exploration.

Figure 5(c) This fractal, constrained within the compact domain of $[-2, 2] \times [-2, 2]$, offers a more concentrated depiction of the Mandelbrot set. The fractal preserves its symmetric properties, presenting a dense and complex pattern centered around the origin. The generation time of 3.952 seconds reflects the computational effort required to detail such a densely packed structure. The gradient in color intensity accentuates both the central details and the boundary formations, providing a comprehensive representation of the set's complexity.

Figure 5(d) This fractal, defined over the largest range $[-3, 3] \times [-2, 2]$, resembles the general appearance of the Mandelbrot set more closely. While slight asymmetries are observable along the horizontal axis, the overall structure maintains its characteristic order. The figure was generated in 3.728 seconds, reflecting the additional computational requirements for a broader domain. The variation in color intensity is particularly effective in emphasizing the curvature of the outer layers and the intricacy of the internal regions.

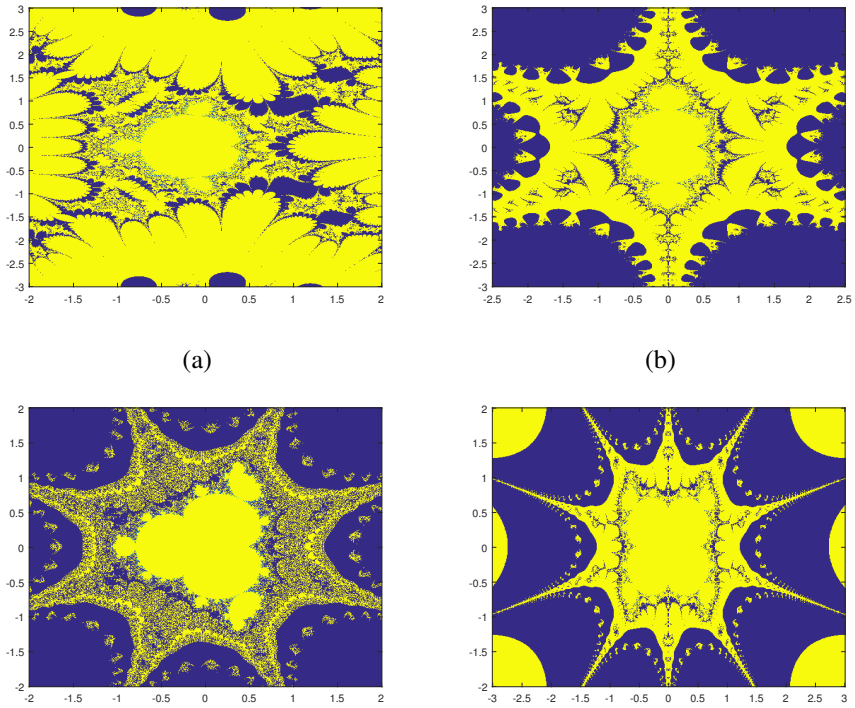

(a) (b)

(c) (d)

Figure 5. Fractals obtained from the Mandelbrot set according to the q values in Table 5.

Table 5. The parameters applied in Figure 5.

Fig. No	a	b	$\mathfrak{c}$	k	$\hbar_1$	$\hbar_2$	$\hbar_3$	q
5(a)	1	0.0001	0.0002	0.0005	0.60	0.70	0.85	2
5(b)	1	0.0001	0.0002	0.0005	0.60	0.70	0.85	3
5(c)	1	0.0001	0.0002	0.0005	0.60	0.70	0.85	4
5(d)	1	0.0001	0.0002	0.0005	0.60	0.70	0.85	5

Figure 6(a) The fractal defined in the domain $[-2, 2] \times [-2, 2]$ exemplifies the characteristic features of the Mandelbrot set, specifically its compact branching patterns and self-similarity. The figure demonstrates clear symmetry along both the vertical and horizontal axes, aligning with well-established representations of the Mandelbrot set. With a generation time of 1.995 seconds, this fractal stands out for its computational efficiency. The gradual variation in color intensity enhances the visibility of the intricate boundary regions and internal structures, aiding in the visual differentiation of its features.

Figure 6(b) This fractal, constructed over the larger domain $[-3, 3] \times [-3, 3]$, offers a broader visualization of the Mandelbrot set, allowing for a more expansive display of its branching complexity. The fractal retains its symmetry along both axes, with the expanded domain contributing to a more comprehensive depiction of its intricate external layers. The generation time of 2.010 seconds is slightly longer than that of Figure 6(a), consistent with the increased domain size. The color transitions are smoother and subtler, emphasizing both the central density and the detailed peripheral structures.

Figure 6(c) The fractal defined over the domain $[-2.5, 2.5] \times [-3, 3]$ represents an intermediate perspective of the Mandelbrot set, balancing compactness and breadth. The fractal displays a near-perfect symmetry along the vertical axis, while horizontal variations are less pronounced but observable. The generation time of 2.091 seconds reflects the additional computational effort required for capturing finer details in this domain. The distribution of color intensity across the structure highlights the dense center and gradually fades outward, underscoring the transition between high-complexity and low-complexity regions.

Figure 6(d) This fractal, covering the domain $[-2.5, 2.5] \times [-2.5, 2.5]$, offers a balanced and detailed representation of the Mandelbrot set, focusing on both the inner and outer features. Symmetry is well-preserved, with uniformity evident along both axes. The computation time of 2.060 seconds indicates a relatively stable performance despite the square domain's slightly larger computational demands. The color intensity variations are finely tuned, accentuating the fractal's intricate inner regions while providing a clear contrast with the outer boundary layers.

Table 6. The parameters applied in Figure 6.

Fig. No	a	b	$\mathfrak{c}$	k	$\hbar_1$	$\hbar_2$	$\hbar_3$	q
6(a)	0.001+0.002i	1.002+0.003i	0.003+0.004i	0.04	0.20	0.50	0.40	2
6(b)	0.05+0.06i	1.001+0.002i	0.001-0.003i	0.08	0.050	0.040	0.030	2
6(c)	0.01+0.01i	1.02+0.02i	3.05+0.03i	0.75	0.04	0.05	0.06	2
6(d)	0.0001i	2.0001+0.0003i	2.0002+0.0002i	0.07	0.35	0.25	0.40	2

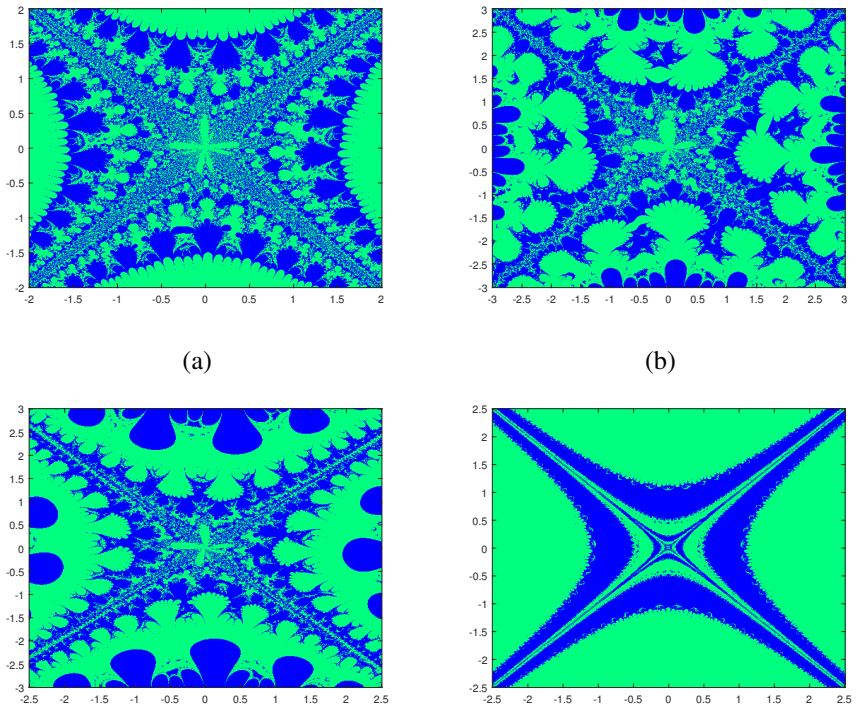

(a) (b)

(c) (d)

Figure 6. Fractals obtained from the Mandelbrot set for varying values of all parameters except q according to Table 6.

Figure 7(a) This fractal, defined in the domain $[-2, 2]\times[-2, 2]$, adheres closely to the well-established properties of the Mandelbrot set. Its symmetric structure along both vertical and horizontal axes is indicative of the set's inherent geometric regularities. The fractal required a computation time of 3.410 seconds, reflecting the intricate details captured within this domain. The color intensity gradients are smoothly distributed, emphasizing the transition from high-complexity regions near the center to less-detailed peripheral areas.

Figure 7(b) This fractal, spanning the extended range of $[-2.5, 2.5] \times [-2.5, 2.5]$, provides a broader representation of the Mandelbrot set. The figure retains strong symmetry along both axes, with the additional domain size allowing for a more comprehensive depiction of the fractal's branching patterns. The generation time of 3.425 seconds is consistent with the increased computational demand of the larger area. The subtle shifts in color intensity effectively highlight the fractal's intricate internal and external structures.

Figure 7(c) This fractal, defined within a narrow domain of $[-1, 1] \times [-2, 2]$, offers a more focused perspective of the Mandelbrot set. The fractal's symmetry is preserved, with the compact domain emphasizing central details while limiting the visualization of the outer regions. The computation time of 3.422 seconds suggests the additional effort required to detail the dense central structures. The color intensity variation is well-applied, concentrating on the intricate core and progressively softening toward the edges.

Figure 7(d) The fractal defined over the expansive domain $[-2.5, 2.5] \times [-3.5, 3.5]$ provides an

extended view of the Mandelbrot set, capturing both its central complexity and peripheral features. The fractal exhibits strong vertical and horizontal symmetry, with slight asymmetries in the outer layers due to domain-specific variations. The computation time of 3.326 seconds is slightly lower, possibly reflecting optimization in generating the outer structures. The color intensity transitions are notably smooth, enhancing the visual differentiation between high-complexity and low-complexity regions.

Table 7. The parameters applied in Figure 7.

Fig. No	a	b	$\mathfrak{c}$	k	$\wp_1$	$\wp_2$	$\wp_3$	q
7(a)	1.02+1.02i	0.002+0.001i	0.03+0.01i	0.10	0.099	0.099	0.099	3
7(b)	1.004+1.004i	0.02+0.05i	1.03+0.02i	0.60	0.04	0.06	0.08	3
7(c)	1.003+0.09i	0.002+0.002i	0.02-0.02i	0.60	0.10	0.10	0.10	3
7(d)	0.002i	1.1+0.1i	0.1+0.1i	0.09	0.39	0.49	0.59	3

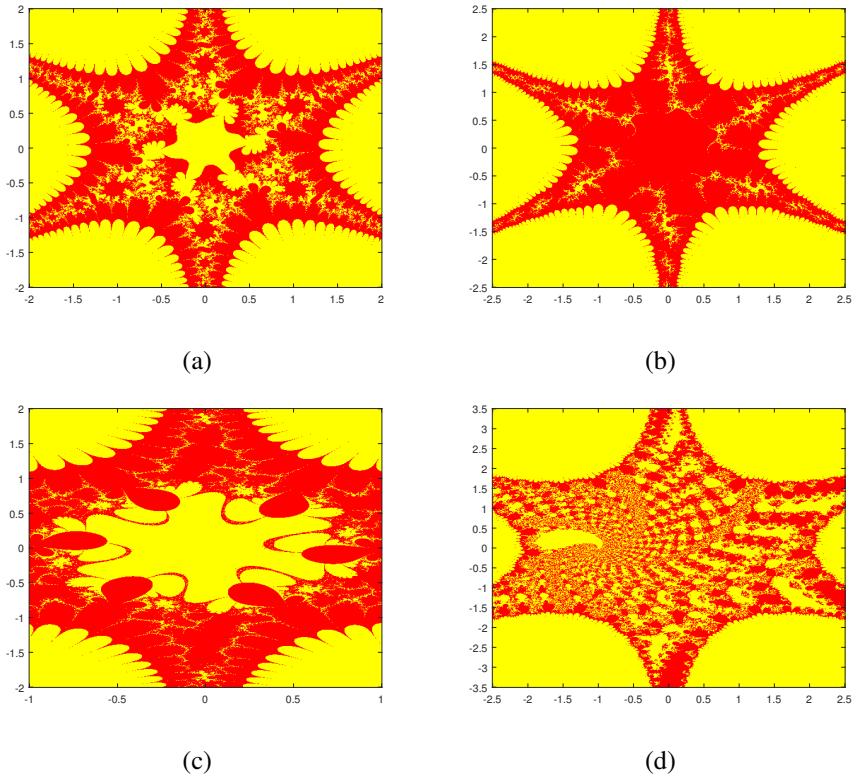

(a) (b)

(c) (d)

Figure 7. Fractals obtained from the Mandelbrot set for varying values of all parameters except q according to Table 7.

Figure 8(a) This fractal, generated over the domain $[-2.5, 2.5] \times [-2.5, 2.5]$, closely aligns with the standard characteristics of the Mandelbrot set. Its symmetry is evident along both vertical and horizontal axes, reflecting the uniformity of its underlying mathematical structure. With a generation time of 2.002 seconds, this fractal demonstrates high computational efficiency. The color intensity transitions are evenly distributed, providing a balanced emphasis on both central

details and boundary regions, which underscores the fractal's intricate nature.

Figure 8(b) It is defined within the same domain as Figure 8(a), highlighting the influence of parameter variation, particularly the value of q. The fractal retains its symmetry but exhibits a more pronounced complexity in its inner structures. The generation time of 4.054 seconds is significantly longer, suggesting a higher computational demand due to the enhanced detail. The color intensity is notably vibrant, particularly in regions of high complexity, accentuating the fractal's intricate branching patterns.

Figure 8(c) The fractal spanning a larger domain of $[-3, 3] \times [-3, 3]$ offers a broader representation of the Mandelbrot set. The fractal displays symmetry along both axes and emphasizes outer structural details, which are less pronounced in Figures 8(a) and 8(b). The computation time of 4.042 seconds reflects the increased computational effort required for capturing the expanded area. The color intensity gradients are subtly varied, emphasizing the transition from dense central regions to sparse outer layers, creating a visually striking effect.

Figure 8(d) This fractal, defined over the domain $[-2.5, 2.5] \times [-3, 3]$, balances the compactness of Figures 8(a) and 8(b) with the broader perspective of Figure 8(c). The fractal maintains strong vertical and horizontal symmetry, with slightly elongated features due to the domain's asymmetry. The generation time of 4.304 seconds, the longest among the four, reflects the added complexity of this domain. The color intensity variations are particularly pronounced, highlighting the fractal's rich internal structures and enhancing the visual distinction between dense and sparse regions.

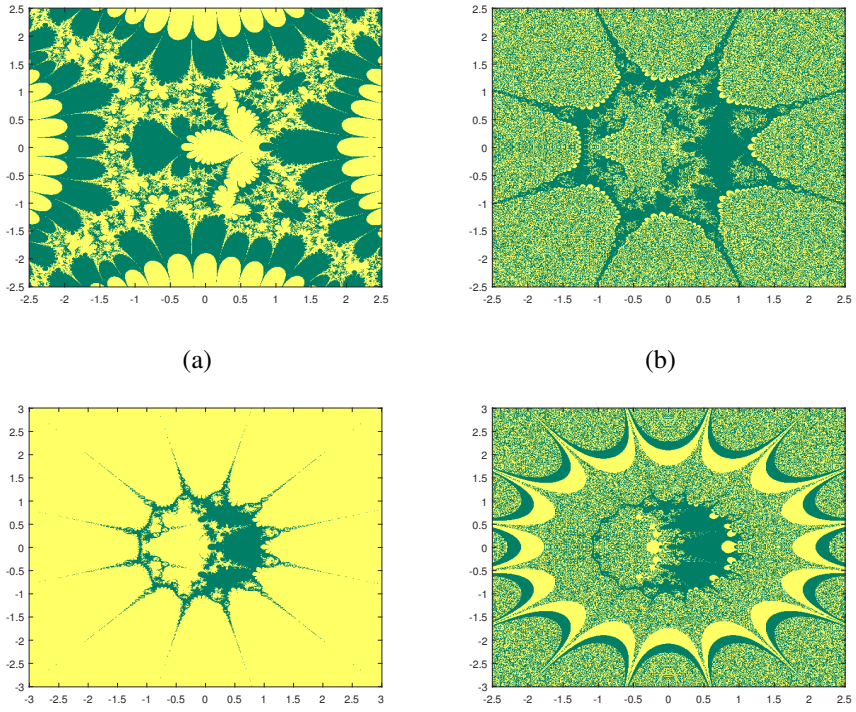

(a) (b)

(c) (d)

Figure 8. Fractals obtained from the Mandelbrot set for different values of q according to Table 8.

Table 8. The parameters applied in Figure 8.

Fig. No	a	b	$\mathfrak{c}$	k	$\wp_1$	$\wp_2$	$\wp_3$	q
8(a)	1.003	1.002	0.001	0.05	0.001	0.009	0.008	2
8(b)	1.003	1.002	0.001	0.05	0.001	0.009	0.008	4
8(c)	1.003	1.002	0.001	0.05	0.001	0.009	0.008	6
8(d)	1.003	1.002	0.001	0.05	0.001	0.009	0.008	8

5. Conclusions

In this study, a three-step, fixed-point iteration method was employed to determine escape criteria for complex-valued hyperbolic sine and complex-valued hyperbolic cosine functions. Additionally, the study examined how the fractals generated using these escape criteria can be shaped based on the constants $a, b, \mathfrak{c}$, and q in the equations, as reflected in the data presented in Tables 1–8. The findings indicate that the choice of q, whether treated as a fixed or variable parameter, plays a critical role in determining the shapes of the resulting fractals (e.g., whether they exhibit circular structures).

It was observed that the color intensity of the fractals increases significantly, particularly when $q = 4$ (see Figures 1(c), 3(c), 5(c), and 8(b)). A similar effect was noted for $q = 8$, as illustrated in Figure 8(d). These results demonstrate that the PMP iteration method exhibits remarkable technical potential in fractal generation, demonstrating notable mathematical precision, structural depth, and algorithmic efficiency. Furthermore, the findings contribute to the growing body of application-oriented theoretical work that integrates fixed-point iteration methods with fractal geometry.

In future work, we aim to investigate the presence of Parrondo's paradox within Mandelbrot and Julia sets of complex hyperbolic sine and cosine functions via PMP orbit. This phenomenon, previously observed in polynomial fractals, suggests that a combination of losing strategies can yield a winning outcome [28]. A comparative analysis with existing studies will be conducted to explore whether a similar behavior exists in this iteration. Additionally, we plan to examine the interplay between h-convexity and the PMP iteration method, focusing on its impact on escape criteria and fractal geometries, which may lead to the discovery of novel fractal structures.

Further research will also address the optimization of parameters such as $a, b, \mathfrak{c}$, and q, evaluating their effects on computational efficiency, symmetry, and color intensity in fractal generation. Moreover, we intend to explore the applicability of these fractals in modeling dynamic systems, particularly in stability and chaos analyses, thereby bridging theoretical advancements in fractal geometry with practical applications in physics and engineering.

Author contributions

Tunçar Şahan: Writing-review & editing, Visualization, Software; Yunus Atalan: Methodology, Investigation, Formal Analysis, Writing-original draft & editing. All authors have read and approved the final version of the manuscript for publication.

Use of Generative-AI tools declaration

The authors declare they have not used Artificial Intelligence (AI) tools in the creation of this article.

Acknowledgments

The authors would like to thank the anonymous reviewers for their careful reading, insightful comments, and helpful suggestions, which improved the presentation of the paper. This work was completed without any financial support from funding sources.

Conflict of interest

The authors declare that there is no conflict of interest regarding the publication of this paper.

References

1. B. B. Mandelbrot, *Les objets fractals: forme, hasard et dimension*, Paris: Flammarion: 1975.
2. M. Rani, V. Kumar, Superior Julia set, *J. Korea Soc. Math. Educ. Ser. D; Res. Math. Educ.*, **8** (2004), 261–277.
3. M. Rani, V. Kumar, Superior Mandelbrot set, *J. Korea Soc. Math. Educ. Ser. D; Res. Math. Educ.*, **8** (2004), 279–291.
4. Y. Wang, Fractional quantum Julia set, *Appl. Math. Comput.*, **453** (2023), 128077. https://doi.org/10.1016/j.amc.2023.128077
5. Y. Wang, S. Liu, H. Li, D. Wang, On the spatial Julia set generated by fractional Lotka-Volterra system with noise, *Chaos Soliton Fract.*, **128** (2019), 129–138. https://doi.org/10.1016/j.chaos.2019.07.044
6. Y. Wang, S. Liu, W. Wang, Fractal dimension analysis and control of Julia set generated by fractional Lotka–Volterra models, *Commun. Nonlinear Sci. Numer. Simul.*, **72** (2019), 417–431. https://doi.org/10.1016/j.cnsns.2019.01.009
7. Y. Wang, S. Liu, Fractal analysis and control of the fractional Lotka-Volterra model, *Nonlinear Dyn.*, **95** (2019), 1457–1470. https://doi.org/10.1007/s11071-018-4638-7
8. M. F. Danca, M. Fečkan, Mandelbrot set and Julia sets of fractional order, *Nonlinear Dyn.*, **111** (2023), 9555–9570. http://dx.doi.org/10.1007/s11071-023-08311-2
9. M. F. Danca, Mandelbrot set as a particular Julia set of fractional order, equipotential lines and external rays of Mandelbrot and Julia sets of fractional order, *Fractal Fract.*, **8** (2024), 69. http://doi.org/10.3390/fractalfract8010069
10. A. Bhoria, A. Panwar, M. Sajid, Mandelbrot and Julia sets of transcendental functions using Picard-Thakur iteration, *Fractal Fract.*, **7** (2023), 768. http://doi.org/10.3390/fractalfract7100768

11. H. Qi, M. Tanveer, W. Nazeer, Y. Chu, Fixed point results for fractal generation of complex polynomials involving sine function via non-standard iterations, *IEEE Access*, **8** (2020), 154301–154317. http://doi.org/10.1109/ACCESS.2020.3018090

12. N. Hamada, F. Kharbat, Mandelbrot and Julia sets of complex polynomials involving sine and cosine functions via Picard-Mann orbit, *Complex Anal. Oper. Theory*, **17** (2023), 13. http://doi.org/10.1007/s11785-022-01312-w

13. S. M. Kang, A. Rafiq, A. Latif, A. A. Shahid, Y. C. Kwun, Tricorns and multicorns of S-iteration scheme, *J. Funct. Spaces*, **2015** (2015), 417167. http://doi.org/10.1155/2015/417167

14. S. Kumari, K. Gdawiec, A. Nandal, M. Postolache, R. Chugh, A novel approach to generate Mandelbrot sets, Julia sets and biomorphs via viscosity approximation method, *Chaos Soliton Fract.*, **163** (2022), 112540. http://doi.org/10.1016/j.chaos.2022.112540

15. A. Tomar, V. Kumar, U. S. Rana, M. Sajid, Fractals as Julia and Mandelbrot sets of complex cosine functions via fixed point iterations, *Symmetry*, **15** (2023), 478. http://doi.org/10.3390/sym15020478

16. A. Murali, K. Muthunagai, Generation of Julia and Mandelbrot fractals for a generalized rational type mapping via viscosity approximation type iterative method extended with s-convexity, *AIMS Math.*, **9** (2024), 20221–20244. http://doi.org/10.3934/math.2024985

17. A. Tassaddiq, General escape criteria for the generation of fractals in extended Jungck-Noor orbit, *Math. Comput. Simul.*, **196** (2022), 1–14. http://doi.org/10.1016/j.matcom.2022.01.003

18. A. Tassaddiq, M. Tanveer, M. Azhar, F. Lakhani, W. Nazeer, Z. Afzal, Escape criterion for generating fractals using Picard-Thakur hybrid iteration, *Alex. Eng. J.*, **100** (2024), 331–339. http://doi.org/10.1016/j.aej.2024.03.074

19. M. Tanveer, W. Nazeer, K. Gdawiec, New escape criteria for complex fractals generation in Jungck-CR orbit *Indian J. Pure Appl. Math.*, **51** (2020), 1285–1303. http://doi.org/10.1007/s13226-020-0466-9

20. R. L. Devaney, *An introduction to chaotic dynamical systems*, 3 Eds., London: Chapman and Hall, 2021. http://doi.org/10.1201/9780429280801

21. D. Peitgen, H. O. Jürgens, D. Saupe, *Chaos and fractals: new frontiers of science*, 2 Eds., New York: Springer, 2004. http://doi.org/10.1007/b97624

22. K. Falconer, *Fractal geometry: mathematical foundations and applications*, Hoboken: John Wiley & Sons, 2003. http://doi.org/10.1002/0470013850

23. M. Schroeder, *Fractals, chaos, power laws: minutes from an infinite paradise*, Mineola: Dover Publications, 1991.

24. D. Wang, Y. Zhang, W. Lou, W. Zang, Fractal viewpoint in supply chain price competition, *Chaos Soliton Fract.*, **176** (2023), 114175. http://doi.org/10.1016/j.chaos.2023.114175

25. R. L. Devaney, *A first course in chaotic dynamical systems: theory and experiment*, 2 Eds., London: Chapman and Hall, 2020. http://doi.org/10.1201/9780429280665

26. M. F. Barnsley, *Fractals everywhere*, 2 Eds., Amsterdam: Elsevier, 1993. http://doi.org/10.1016/C2013-0-10335-2

27. V. Karakaya, Y. Atalan, K. Dogan, N. E. H. Bouzara, Some fixed point results for a new three steps iteration process in Banach spaces, *Fixed Point Theory*, **18** (2017), 625–640. http://doi.org/10.24193/fpt-ro.2017.2.50

28. Y. Zhang, D. Wang, Fractals Parrondo's Paradox in alternated superior complex system, *Fractal Fract.*, **5** (2021), 39. http://doi.org/10.3390/fractalfract5020039

AIMS Press